NASA Technical Memorandum 84524

APPLICATION OF MATRIX SINGULAR VALUE PROPERTIES FOR EVALUATING GAIN AND PHASE MARGINS OF MULTILOOP SYSTEMS

V. MUKHOPADHYAY AND J. R. NEWSOM

JULY 1982

National Aeronautics and Space Administration

Langley Research Center
Hampton, Virginia 23665

APPLICATION OF MATRIX SINGULAR VALUE PROPERTIES FOR EVALUATING GAIN AND PHASE MARGINS OF MULTILOOP SYSTEMS

V. Mukhopadhyay
George Washington University
Joint Institute for Advancement of Flight Sciences
Hampton, Virginia 23665

and

J. R. Newsom
NASA Langley Research Center
Hampton, Virginia 23665

Abstract

A stability margin evaluation method in terms of simultaneous gain and phase changes in all loops of a multiloop system is presented. A universal gain-phase margin evaluation diagram is constructed by generalizing an existing method using matrix singular value properties. Using this diagram and computing the minimum singular value of the system return difference matrix over the operating frequency range, regions of guaranteed stability margins can be obtained. Singular values are computed for a wing flutter suppression and a drone lateral attitude control problem. The numerical results indicate that this method predicts quite conservative stability margins. In the second example if the eigenvalue magnitude is used instead of the singular value, as a measure of nearness to singularity, more realistic stability margins are obtained. However, this relaxed measure generally cannot guarantee global stability.

Nomenclature

A,B,C,D	control law quadruple matrices
$\bar{A},\bar{B},\bar{C}$	augmented system dynamics, input and output matrices, respectively
dB	decibel
F,G_u,H	plant dynamics, input and output matrices, respectively
F_a	augmented system closed loop matrix
G	open loop transfer matrix
I	identity matrix
j	$\sqrt{-1}$
k_n	n^{th} loop gain in L matrix
L	diagonal gain and phase change matrix
M	order of control law
N_s,N_c,N_o	order of plant, input and output vectors respectively
p	a parameter
$r,\bar{r}$	reference signal and its amplitude
s	Laplace variable
T_u,T_y	transfer matrix relating $\bar{r}$ to $\bar{u}$ and $\bar{y}$, respectively
$u,\bar{u}$	plant input and its amplitude
u_i,v_i	left and right eigenvectors
x_a	augmented state vector
x_c	controller state vector
x_s	plant state vector
$y,\bar{y}$	feedback signal and its amplitude
z	plant output vector
β	sideslip angle (deg.)
δ_1,δ_2	elevon and rudder actuator state vectors, respectively (deg.)
$\underline{\lambda}(\ )$	eigenvalue of matrix ( )
$\bar{\lambda},\underline{\lambda}$	maximum and minimum eigenvalue
$\bar{\sigma}(\ ),\underline{\sigma}(\ )$	maximum and minimum singular value, respectively, of matrix ( )
ϕ_n	n^{th} loop phase in L matrix (deg)
$\phi,\dot{\phi}$	roll angle and rate (deg/sec)
$\psi,\dot{\psi}$	yaw angle and rate (deg/sec)
ω	frequency
$\lvert\ \rvert$	magnitude
$\lVert\ \rVert$	Euclidean norm
$[\ ]^*$	complex conjugate transpose of [ ]
$[\ ]^T$	transpose of [ ]
$\dot{(\ )}$	represents time derivative of ( )

Introduction

Robustness criteria of multi-input multi-output (MIMO) feedback control systems using matrix singular value properties and their relation to the classical gain and phase margins have been a subject of research in recent years.[1-4] In a multiloop system, the classical single loop Nyquist tests are not adequate for gain or phase margin evaluation since the gain or phase is changed in one loop at a time. Using the minimum singular value of the system return difference matrix, criteria were developed in reference 4 for predicting guaranteed stability margins of multiloop systems in terms of either gain or phase change in all feedback loops. In this paper, the above method is generalized to include simultaneous gain and phase change in all loops. A universal gain-phase margin evaluation diagram is constructed. Using this diagram and computing the minimum singular value of the system return difference matrix over the operating frequency range, regions of guaranteed gain and phase margins can be obtained. Using this study and a singular value gradient expression derived herein, one can develop an algorithm for a direct design of robust multiloop control laws using the concept of cumulative constraint and multi-objective optimization.[5-6]

Singular values are computed for two examples for better understanding and evaluation of their relation to stability margins. The first example is a 29th order single-input single-output (SISO) system which represents an aeroelastic wind-tunnel wing model with a flutter suppression system. In reference 7 two flutter suppression control laws were synthesized that provided different degrees of robustness (gain and phase margins). These two control laws are examined using a classical Nyquist diagram and the singular value analysis. The correspondence between the stability margins predicted by the two methods are discussed.

The second example is an 8th order two-input two-output system which represents an experimental drone aircraft[8] with a lateral attitude control system. The phase and gain margins from classical single-loop tests and the singular value approach are determined and compared with the actual stability boundary. The plot of the return difference matrix eigenvalue in the complex plane is also studied. This plot provides useful qualitative gain and phase margin information not contained in singular values.

Analysis

Problem Formulation

Let a multiloop feedback control system be described by the set of constant coefficient state-space equations (1) to (5).

Plant

$$\dot{x}_s = Fx_s + G_u u \tag{1}$$

$$z = Hx_s \tag{2}$$

Control Law

$$\dot{x}_c = Ax_c + Bz \tag{3}$$

$$y = -[Cx_c + Dz] \tag{4}$$

Interconnection

$$u = r - y \tag{5}$$

Equation (1) represents an N_s^{th} order plant having N_0 output measurements z modeled by equation (2) and N_c control inputs u. Equations (3) and (4) represent an M^{th} order feedback control law driven by the sensor output z. The reference input signal is r. In terms of a transfer function, the sensor output and the control laws are

$$z = [H(Is - F)^{-1}G_u]u \tag{6}$$

$$u = [C(Is - A)^{-1}B + D]z + r \tag{7}$$

respectively. Here s is the Laplace variable. Figure 1 shows the block diagram of a multiloop system with unity feedback in which a square diagonal matrix L is introduced at the plant input u to examine the system gain and phase margins.

$$L = \text{Diag}[k_n \exp(j\phi_n)] \tag{8}$$

$$n = 1,2,\ldots N_c$$

At nominal conditions, $k_n = 1$ and $\phi_n = 0$ for all n and therefore L is the identity matrix. In a traditional single loop test, either k_n or ϕ_n is changed in one loop at a time. The gain or phase margin of the loop is defined as the smallest change in k_n or ϕ_n respectively from the nominal value for which the closed loop system remains stable. However, it would be more desirable to find the range in which both k_n and ϕ_n can be changed simultaneously in all loops for which the system would remain stable. This is our present objective.

The stability can always be detected in the time domain by computing the eigenvalues of the closed loop system dynamic matrix

$$F_a = \left[\begin{array}{c|c} F + G_u LDH & G_u LC \\ \hline BH & A \end{array}\right] \tag{9}$$

and examining the sign of the real part of the eigenvalues. Traditionally in single loop system design, the stability margins are evaluated as a gain or phase margin in the frequency domain using Nyquist diagrams. In a multiloop system, a frequency domain analysis may be formulated as follows.

Write equations (1) to (5) and (8) in an augmented form as

$$\dot{x}_a = \bar{A}x_a + \bar{B}Lu \tag{10}$$

$$u = -\bar{C}x_a + r \tag{11}$$

where

$$x_a = \begin{Bmatrix} x_s \\ x_c \end{Bmatrix} \qquad \bar{A} = \left[\begin{array}{c|c} F & 0 \\ \hline BH & A \end{array}\right] \tag{12}$$

$$\bar{B} = \begin{bmatrix} G_u \\ \hline 0 \end{bmatrix} \qquad \bar{C} = -[DH \mid C]$$

Using equations (10) and (11), the plant input u and control output y can be written as functions of r in Laplace domain as

$$u = (I + G(s)L)^{-1}r \tag{13}$$

$$y = G(s)L(I + G(s)L)^{-1}r \tag{14}$$

where $G(s) = \bar{C}(Is - \bar{A})^{-1}\bar{B}$ (15)

Using equations (6) and (7) one can also arrive at the relation (13) and (14) in which

$$G(s) = -[C(Is - A)^{-1}B + D]$$
$$[H(Is - F)^{-1}G_u] \tag{16}$$

Equations (15) and (16) can be shown to be identical. The transfer function matrix $[I+G(s)]$ is defined as the system return difference matrix for nominal gain (i.e., $L = I$). For a steady unit sinusoidal input reference signal r, one can always compute $[I+G(j\omega)]$ over the range of operating frequency ω. The multivariable system is not robust to modeling errors if $[I+G(j\omega)]$ is nearly singular at some critical frequency ω_c. One can plot the determinant of $[I+G(j\omega)]$ in the complex plane and monitor its closeness to zero as it encircles the origin. But one cannot get a satisfactory notion of stability margin directly from the determinant locus because the closeness of a matrix to singularity cannot always be detected in terms of its determinant[4].

However, matrix singular values or principal gains are related to the system input-output magnitudes governed by equations (13) and (14) in the frequency domain,[2,3] and its properties are suitable to relate them to the stability margins. These properties are briefly reviewed next for later use.

Review of Matrix Singular Value Properties

Consider a sinusoidal input reference signal $r = \bar{r}e^{j\omega t}$ for which the steady state input u and output y are given by $\bar{u}e^{j\omega t}$ and $\bar{y}e^{j\omega t}$. The complex amplitudes $\bar{u}$, $\bar{y}$ and $\bar{r}$ are related by the complex matrix relations

$$\bar{u} = T_u(j\omega)\bar{r} \tag{17}$$

$$\bar{y} = T_y(j\omega)\bar{r} \tag{18}$$

where $$T_u = [I + G(j\omega)L]^{-1} \tag{19}$$

$$T_y = G(j\omega)L[I + G(j\omega)L]^{-1}$$

$$= [I + (G(j\omega)L)^{-1}]^{-1} \tag{20}$$

For convenience the argument $(j\omega)$ will be omitted in the rest of the paper except when necessary. A scalar measure of amplitude of $\bar{u}$ is

$$\sqrt{u^*u} = \sqrt{r^*[T_u^*T_u]r} \tag{21}$$

where superscript * indicates complex conjugate transpose of a vector or matrix. The maximum and minimum singular values of T_u provide a measure of the upper and lower bound of T_u in the sense

$$\max\sqrt{\frac{r^*[T_u^*T_u]r}{r^*r}} \equiv \|T_u\|_{max} = \bar{\sigma}(T_u) \tag{22}$$

$$\min\sqrt{\frac{r^*[T_u^*T_u]r}{r^*r}} \equiv \|T_u\|_{min} = \underline{\sigma}(T_u) \tag{23}$$

The maximum and minimum singular values, denoted by $\bar{\sigma}$ and $\underline{\sigma}$, are given by the positive square root of the maximum and minimum eigenvalues of $T_u^*T_u$ (or $T_uT_u^*$). The response amplitude bounds hold true not only for sinusoidal inputs but also for aperiodic and stochastic input signals.[2] Other important properties of singular values are

$$\bar{\sigma}(G)\bar{\sigma}(L) \geq \bar{\sigma}(GL) \tag{24}$$

$$\bar{\sigma}(G) \geq |\lambda(G)| \geq \underline{\sigma}(G) \tag{25}$$

If $\underline{\sigma}(G) = 0$ then G is singular (26)

If G^{-1} exists $\bar{\sigma}(G) = 1/\underline{\sigma}(G^{-1})$ (27)

If G is nonsingular, then a sufficient condition for $(G + L)$ to remain nonsingular is

$$\bar{\sigma}(L) < \underline{\sigma}(G) \tag{28}$$

Here G and L are any compatible square matrices and $\lambda(G)$ denotes any eigenvalue of G. Using these properties and generalizing the analysis presented in reference 4, it is possible to construct a universal gain-phase margin evaluation diagram as described in the following section.

Universal Gain and Phase Margin Diagram

Since the closed loop system is assumed to be stable for nominal gain (i.e., L=I), the complex matrix T_u must exist. This implies

$$\underline{\sigma}(I+G) > 0 \tag{29}$$

The smallest singular value of the return difference matrix over the operating frequency range is a measure of stability margin. The objective of this section is to relate this to the maximum range of variation of k_n and ϕ_n in the matrix L from their nominal values for which the perturbed system remains stable, i.e.

$$\underline{\sigma}(I+GL) > 0 \tag{30}$$

It can be shown that the stability of the perturbed system is guaranteed if

$$\bar{\sigma}(L^{-1}-I) < \underline{\sigma}(I+G) \tag{31}$$

assuming L^{-1} exists[4]. The basic reasoning is as follows. Since L^{-1} and $(I+G)^{-1}$ exists, rewrite $I+GL$ to separate L from the G matrix, as

$$I+GL = [(L^{-1}-I)(I+G)^{-1}+I](I+G)L \tag{32}$$

Since $(I+G)$ and L are assumed to be nonsingular, $(I+GL)$ is nonsingular if and only if $[(L^{-1}-I)(I+G)^{-1}+I]$ is nonsingular. Condition (31) guarantees that

$$\|[(L^{-1}-I)(I+G)^{-1}]\|_{max} < 1$$

or

$$\bar{\sigma}[(L^{-1}-I)(I+G)^{-1}] < 1 \tag{33}$$

which ensures that $[(L^{-1}-I)(I+G)^{-1}+I]$ is nonsingular. In arriving at equation (33), the inequality conditions (24), (28) and equation (27) are used. Note that this is a conservative condition, and it is possible to construct an L matrix which violates this condition, yet fails to destabilize the system.

If we consider simultaneous gain and phase changes in every loop using the L matrix given by equation (8), then

$$\max\bar{\sigma}(L^{-1}-I) = \sqrt{(1-\frac{1}{k_n})^2 + \frac{2}{k_n}(1-\cos\phi_n)} \tag{34}$$

for all n with $k_n>0$. Reference 4 considers only the classical cases of gain or phase changes keeping $\phi_n = 0$ or $k_n=1$, respectively. Using equation (34), the general case of simultaneous gain and phase changes can be examined. Equation (34) is presented in Fig. 2 as a universal diagram for gain and phase margin evaluation. For example if the smallest $\underline{\sigma}(I+G)$ for a system is 0.6 then the closed loop system will tolerate simultaneous gain and phase changes of -1.5dB to +5.3dB, and -30° to +30°, respectively in all input loops. In a classical sense, when either gain or phase is changed, the margins are -4.2dB and +8dB or ±35°, respectively.

Using equation (34) the condition (31) can also be depicted as a plot of gain margin versus phase margin with smallest $\underline{\sigma}(I+G)$ as a parameter. This is shown in Fig. 3 to indicate regions of guaranteed stability. If the phase and gain changes k_n and ϕ_n are within the elliptic stability regions for a particular $\underline{\sigma}(I+G)$, then the closed loop system must be stable. For example, if $\underline{\sigma}(I+G) \geq 0.7$ for all frequencies and $\pm 30°$ phase margins are required in all loops then guaranteed simultaneous gain margins are -2.6dB and +8.5dB, i.e., both the phase and gain can be changed in all loops in any manner within these limits, without destabilizing the closed loop system.

From Figs. 2 and 3 it is also easy to verify the well-known result that for a Linear Quadratic Optimal state feedback problem the guaranteed gain margins are -6dB and $+\infty$dB and phase margins are $\pm 60°$ since $\underline{\sigma}(I+G) \geq 1$ (see ref. 4). When both gain and phase changes are considered, for a given phase margin the corresponding gain margins can be established from Figs. 2 and 3.

Computation of Singular Value and Derivative

Since the frequency domain singular value analysis requires inversion of a large matrix $(j\omega - \bar{A})$ at a large number of frequencies (see equation (15)) an efficient computational method[9,10] is used. The basic idea is to transform $\bar{A}$ into an upper Hessenberg matrix so that for all ω, $(j\omega - \bar{A})$ remains in upper Hessenberg form and the inversion problem $(j\omega - \bar{A})^{-1}\bar{B}$ can be solved quickly by simple forward and backward substitution. Thus repeated upper and lower triangular transformations at each ω is avoided.

The complex matrix $(I+G)$ is of small order when multivariable systems involve only a few loops. It is possible to compute the singular value derivatives with respect to control law parameters with minimal additional computation and use them for direct design of robust multiloop control laws using the concept of multiobjective optimization and cumulative constraints[5,6]. The expressions for singular value derivatives are similar to those of eigenvalue derivatives and are presented in appendix A.

Examples

Singular values are computed for two examples for better understanding and evaluation of their relation to stability margins. In the first example involving a single loop flutter suppression system,[7] the correspondence between the classical Nyquist diagram and the singular value plot are examined. Next a two input, two output system describing a drone aircraft[8] with a lateral attitude control system is analyzed in detail.

29th Order Flutter Suppression System (SISO)

In reference 7, 4th order flutter suppression control laws were synthesized for a 25th order state space system representing an aeroelastic wind-tunnel wing model. Two control laws were synthesized that provided different stability margins. The transfer functions for these two control laws are:

Control Law (a)

$$\frac{u}{z} = \frac{(-364.4)(s-136.4)(s^2+73.69s + 5697)}{(s+2.057)(s+2057)(s^2+46.37s + 2047)} \quad \frac{\text{deg}}{\text{g}}$$

Control Law (b)

$$\frac{u}{z} = \frac{(1939.4)(s+24.74)(s^2+87.63s + 13806)}{(s+3.864)(s+3270)(s^2+20.97s + 1423)} \quad \frac{\text{deg}}{\text{g}}$$

Nyquist diagrams of the open loop transfer matrix G(s) are presented in Fig. 4. For control law (a) the gain margins are -4.1 dB and 2.6 dB and the phase margins are -22° and +41°. For control law (b) which is comparatively robust, the gain margins are -5.0 dB and +12.3 dB, and the phase margins are -53° and +46°.

A plot of the minimum singular value of $(I+G)$ as a function of frequency with control law (a) and (b) are presented in Fig. 5. The points A, B, C and D on Fig. 5 correspond to the points on Fig. 4 where classical gain and phase margins are defined. If the singular values at point A, B, C and D are used with Fig. 2, the gain and phase margins are determined to be identical to those determined from Fig. 4. However, the minimum singular value occurs at a slightly different point denoted by E. If the singular value at point E (0.23 for control law (a) and 0.69 for control law (b)) is used with Fig. 2 the guaranteed gain or phase margins are determined to be -1.8 dB, +2.3 dB, or ±14° for control law (a) and -4.6 dB, +10.2 dB, or ±40° for control law (b) respectively. When point E is located in the Nyquist locus in Fig. 4, the worst direction of simultaneous gain and phase change are found to be +1.9 dB and -8.0° for control law (a) and -3.3 dB and +24° for control law (b) respectively. These values can be verified using Fig. 2. For this example the singular value plot of Fig. 5 indicates only that control law (b) is more robust than control law (a). If the robustness is characterized by conventional gain and phase margins, quite conservative margins in certain gain or phase directions are obtained by the singular value approach. For realistic margins and information about the worst direction of gain and phase change, the Nyquist diagram is necessary. The Nyquist diagram in the SISO case is equivalent to plotting the eigenvalue of G versus frequency in the complex plane. Also $\lambda(I+G) = 1+\lambda(G)$. Thus qualitative gain and phase margin information may be obtained for the MIMO case by plotting the complex eigenvalues of $(I+G)$. This conjecture is examined in the next MIMO example.

8th Order Drone Lateral Attitude Control System (MIMO)

Figure 6 shows the block diagram of the lateral attitude control system of a drone aircraft.[8] The plant state vector x_s is defined as

$$x_s = \lfloor \beta \ \dot{\phi} \ \dot{\psi} \ \phi \ \delta_1 \ \delta_2 \rfloor^T$$

The plant matrices, F, G, and H, as defined in Eqs. (1) and (2) are given in table 1. The control law matrices A, B, C, and D as defined by Eqs. (3) and (4) are given in table 2. The eigenvalues of plant $\lambda(F)$ are given in table 3. The eigenvalue at $\lambda = 0.1889 \pm j1.051$ results

in an unstable Dutch roll mode. The elements of the input vector $\{u_1\ u_2\}^T$ are the elevon and rudder actuator servo commands respectively. All gain and phase changes are considered at the points denoted by X in figure 6. Figure 7 shows the Nyquist diagrams from classical loop breaking tests at the elevon loop and rudder loop respectively. From this diagram, the gain margin is 27.5 dB and the phase margin is -83.0° for the elevon loop designated as loop 1. For the rudder loop, the gain margins are -4.6 dB and +∞ dB and the phase margins are +55° and -50.5°. This is the primary loop which stabilizes the Dutch roll mode and is designated as loop 2.

Although the single loop values are often used as a measure of loop robustness, they may be inadequate to detect the overall system's weakness to simultaneous gain and phase changes in all loops or to unstructured uncertainties. To study this for the present two-loop problem, the minimum singular value of the return difference matrix ($\underline{\sigma}(I+G)$) over the operating frequency range is plotted in Fig. 8. The minimum singular value is also the lower bound of the minimum eigenvalue magnitude $|\underline{\lambda}(I+G)|$ which is also plotted in Fig. 8. The $\underline{\sigma}$ is constant at 0.35 over low frequencies then drops to its lowest value of 0.25 near 1.2 rad/sec which is close to the frequency of the unstable open loop pole. The $\underline{\sigma}$ increases sharply at higher frequencies and reaches unity value asymptotically. Thus using the stability condition in Eq. (31), the stability is guaranteed if the L matrix has the property $\bar{\sigma}(L^{-1}-I)$ <0.25. If the L matrix is structured as in Eq. 8 which represents gain and phase changes in each loop, then by using Fig. 2, the guaranteed gain margins are found to be -2.0 dB and +2.5 dB. This means k_1 and k_2 can be changed from 0.8 to 1.33 (with $\phi_1 = \phi_2 = 0$) in any manner without destabilizing the system. Similarly ϕ_1 and ϕ_2 can be changed between -15° and +15° (with $k_1=k_2=1$) without encountering instability. If both gain and phase are changed, one can again establish guaranteed gain margins for a given phase margin using Fig. 2 or 3. For example if the ϕ_1 and ϕ_2 variation is between -10° and 10°, the k_1 and k_2 can be varied between 0.85 and 1.25 with guaranteed stability.

The guaranteed stability margins and actual stability boundary for variations in k_1 and k_2 are compared in Fig. 9. The box ABDC indicates the regions of guaranteed stability predicted from the minimum singular value. The curve IJ indicates the actual stability boundary obtained by computing the eigenvalues of matrix F_a in Eq. 9 for many k_1 and k_2 and plotting the eigen-loci. The values of k_1 and k_2 where the real part of any eigenvalue is zero determines one point on the IJ curve. Figure 10 shows the same comparison when only ϕ_1 and ϕ_2 are varied. The actual stability boundary IJ is obtained by computing the determinant of $[I+G(j\omega)]$ for many ϕ_1 and ϕ_2. On the boundary both the real and imaginary parts of the determinant are zero. The actual boundary can also be obtained by the eigen-loci method. Note in Fig. 10 that phase margin predictions from single loop Nyquist tests (Fig. 7) are inadequate when simultaneous phase changes are considered. However, if the robustness is characterized for design purposes by simultaneous gain or phase change tolerances at the input (Figs. 9 and 10) the singular value based gain or phase margin predictions are quite conservative, particularly in certain gain or phase change directions.

In this example it is noted that considerable realistic but qualitative information about gain and phase margins can be obtained from the eigenvalues of (I+G) matrix, which is plotted in the complex plane in Fig. 11. Note that the minimum eigenvalue magnitude $|\underline{\lambda}(I+G)|$ plot in Fig. 8 represents the radial distance of the eigenvalue closest to the origin and is a measure of the closeness of (I+G) to singularity in a limited sense, i.e., for equal diagonal perturbation in the L matrix. If k_1 and k_2 are reduced simultaneously to 0.54, the eigen-diagram in Fig. 11 shrinks radially about the point 1.0 without rotation and point C reaches the origin making the system unstable. Similarly both k_1 and k_2 can be increased indefinitely without encountering instability. If ϕ_1 and ϕ_2 are changed simultaneously from zero to -38°, the diagram rotates about point 1.0 without distortion and point B reaches the origin making the system unstable. Likewise ϕ_1 and ϕ_2 can be increased simultaneously to +65° before point A reaches the origin. These specific stability boundary points can be verified from the actual stability boundary in Figs. 9 and 10. Although nothing can be said regarding stability from Fig. 11 when gain or phase changes are unequal, it does provide qualitative information about the best and worst directions in gain or phase change. This useful design information cannot be obtained from singular value analysis.

It is noted from Fig. 8 (as well as from Fig. 11) that the lowest $|\underline{\lambda}|$ is 0.65 which occurs at a frequency of 1.54 rad/sec. Now if we are allowed to use the minimum eigenvalue magnitude, $|\underline{\lambda}(I+G)|$, instead of the minimum singular value, $\underline{\sigma}(I+G)$, as a measure of nearness to singularity of the (I+G) matrix, then from Fig. 2 the relaxed gain margins are -4.4 dB and +9 dB. This means k_1 and k_2 can be changed in any manner between 0.6 and 2.8. Similarly from Fig. 2, the relaxed phase margins are determined to be ±38°. These two margins are plotted in Fig. 9 and 10, respectively, and are denoted by the box EFHG. Comparison with the actual stability boundary IJ indicates that these eigenvalue magnitude based predictions are more realistic. However, near the edge GH in Fig. 9 the relaxed boundary crosses over into the unstable region. The primary reason for this is that the inequality relation in Eq. (24) does not always hold true if singular values are replaced by eigenvalue magnitude. Hence, one cannot deduce Eq. (33) from Eq. (31) for eigenvalue magnitude except when all elements of a diagonal L matrix are equal. Thus the relaxed stability margin predictions using the condition

$$|\bar{\lambda}(L^{-1}-I)| < |\underline{\lambda}(I+G)|$$

generally cannot guarantee global stability.

Conclusions

A stability margin evaluation method for a multiloop system is presented by generalizing an existing procedure. The method involves computing the singular values of the system return difference matrix over the operating frequency

range. The minimum singular value is related to the stability margins in terms of simultaneous gain and phase changes in all loops. Singular values are computed for two examples for better understanding and evaluation of their relation to stability margins. In the first example involving a single loop flutter suppression system of a wing, the correspondence between the classical Nyquist diagram and the singular value plot is examined. Next a two loop lateral attitude control system of a drone aircraft is examined in detail. Comparison with actual stability regions indicate that the minimum singular value based predictions are quite conservative. If the eigenvalue magnitude is used instead of the singular value as a measure of nearness to singularity more realistic stability margins are obtained for this example. However, this relaxed measure generally cannot guarantee global stability. The plot of the return difference matrix eigenvalues in the complex plane provides useful qualitative gain and phase margin information not contained in singular values.

References

1. Doyle, J. C.; and Stein, G.: Multivariable Feedback Design: Concepts for a Classical/ Modern Synthesis. IEEE Trans. Auto. Control, Vol. AC-26, No. 1, Feb. 1981, pp. 4-16.

2. Postlethwaite, I.; Edmunds, J. M.; and Macfarlane, A. G. J.: Principal Gains and Principal Phases in the Analysis of Linear Multivariable Feedback Systems. IEEE Trans. Auto. Control, Vol. AC-26, No. 1, Feb. 1981, pp. 32-46.

3. Safonov, M. G.; Laub, A. J.; and Hartmann, G. L.: Feedback Properties of Multivariable Systems: The Role and Use of the Return Difference Matrix. IEEE Trans. Auto. Control, Vol. AC-26, No. 1, Feb. 1981, pp. 47-65.

4. Lehtomaki, N. A.; Sandell, N. S., Jr.; and Athans, M.: Robustness Results in Linear Quadratic Gaussian Based Multivariable Control Designs. IEEE Trans. Auto. Control, Vol. 26, No. 1, Feb. 1981, pp. 75-92.

5. Greene, W. H.; and Sobieszczanski-Sobieski, J.: Minimum Mass Sizing of a Large Low-Aspect Ratio Airframe for Flutter-Free Performance. Journal of Aircraft, Vol. 19, No. 3, March 1982, pp. 228-234.

6. Schy, A. A.; and Giesy, D. P.: Multiobjective Insensitive Design of Airplane Control Systems with Uncertain Parameters. AIAA Paper No. CP-81-1818, August 1981.

7. Mukhopadhyay, V.; Newsom, J. R.; and Abel, I.: A Method for Obtaining Reduced Order Control Laws for High Order Systems Using Optimization Techniques. NASA TP 1876, August 1981.

8. Abel, I.; and Newsom, J. R.: Overview of Langley Activities in Active Controls Research. NASA TM 83149, June 1981.

9. Laub, A. J.: Efficient Multivariable Frequency Response Computations. IEEE Trans. Auto. Control, Vol. AC-26, No. 2, April 1981, pp. 407-408.

10. Peters, G.; and Wilkinson, J. H.: Eigenvectors of Real and Complex Matrices by LR and QR Triangularizations. Numerische Mathematik, Vol. 16, No. 3, 1970, pp. 181-204.

Appendix A

Consider a general complex matrix G whose singular values are σ_i and the corresponding right and left normalized eigenvectors are v_i and u_i, respectively. Hence by definition

$$Gv_i = u_i\sigma_i \tag{A1}$$

$$G^*u_i = v_i\sigma_i \qquad i = 1, 2, \ldots N_c \tag{A2}$$

The normalized eigenvectors satisfy the following orthogonal properties.

$$u_i^*u_j = \delta_{ij} \qquad v_i^*v_j = \delta_{ij} \tag{A3}$$

δ_{ij} is the Kroneker delta which is unity when $i=j$ and zero when $i\neq j$. Let p be a parameter for which derivative information is needed. Differentiating equation (A1) and (A2) with respect to p and then premultiplying the result by u_i^* and v_i^*, respectively and adding them together, one obtains

$$u_i^*\frac{\partial G}{\partial p}v_i + v_i^*\frac{\partial G^*}{\partial p}u_i + (u_i^*G - v_i^*\sigma_i)\frac{\partial v_i}{\partial p}$$

$$+ (v_i^*G^* - u_i^*\sigma_i)\frac{\partial u_i}{\partial p} = \frac{\partial \sigma_i}{\partial p}(u_i^*u_i + v_i^*v_i) \tag{A4}$$

Using equations (A1) to (A3) in (A4), one obtains

$$\frac{\partial \sigma_i}{\partial p} = \frac{1}{2}\left(u_i^*\frac{\partial G}{\partial p}v_i + v_i^*\frac{\partial G^*}{\partial p}u_i\right)$$

$$= \text{real part of } \left[u_i^*\frac{\partial G}{\partial p}v_i\right] \tag{A5}$$

Table 1 Plant matrices F, G_u and H for drone lateral attitude control system

$$F = \begin{bmatrix} -.08527 & -0.0001423 & -0.9994 & 0.04142 & 0 & 0.1862 \\ -46.86 & -2.757 & 0.3896 & 0 & -124.3 & 128.6 \\ -0.4248 & -0.06224 & -0.06714 & 0 & -8.792 & -20.46 \\ 0 & 1 & 0 & 0 & 0 & 0 \\ 0 & 0 & 0 & 0 & -20.0 & 0 \\ 0 & 0 & 0 & 0 & 0 & -20.0 \end{bmatrix}$$

$$G = \begin{bmatrix} 0 & 0 \\ 0 & 0 \\ 0 & 0 \\ 0 & 0 \\ 1 & 0 \\ 0 & 1 \end{bmatrix} \qquad H = \begin{bmatrix} 0 & 1 & 0 & 0 & 0 & 0 \\ 0 & 0.07 & 1 & 0 & 0 & 0 \end{bmatrix}$$

Table 2 Control law matrices A, B, C and D for drone lateral attitude control system

$$A = \begin{bmatrix} 0 & 0 \\ 0 & -2 \end{bmatrix} \qquad B = \begin{bmatrix} 1 & 0 \\ 0 & 1 \end{bmatrix}$$

$$C = \begin{bmatrix} 0.1491 & 0 \\ 0 & -4.116 \end{bmatrix} \qquad D = \begin{bmatrix} 0 & 0 \\ 0 & 2.058 \end{bmatrix}$$

Table 3 The eignevalues of the plant, $\lambda(F)$

-0.03701	spiral mode
0.1889 ± j 1.051	Dutch roll (unstable)
-3.25	roll convergence
-20.0	elevon actuator
-20.0	rudder actuator

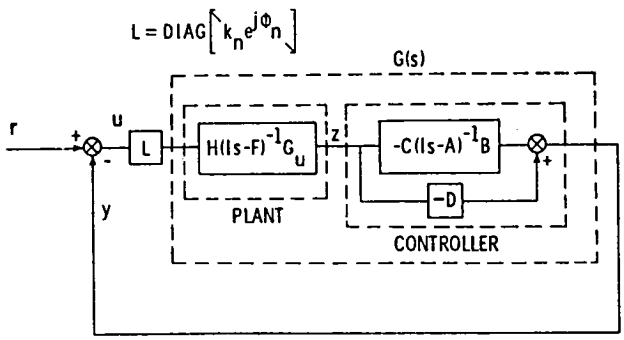

Fig. 1 Block diagram of a multi-input multi-output feedback control system with gain and phase change matrix at the input.

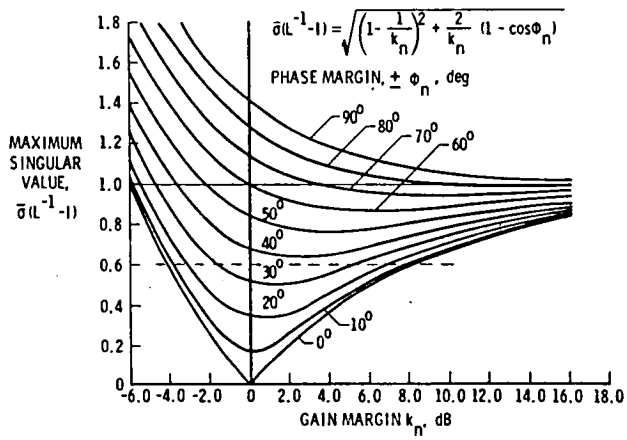

Fig. 2 Universal diagram for multiloop gain-phase margin evaluation.

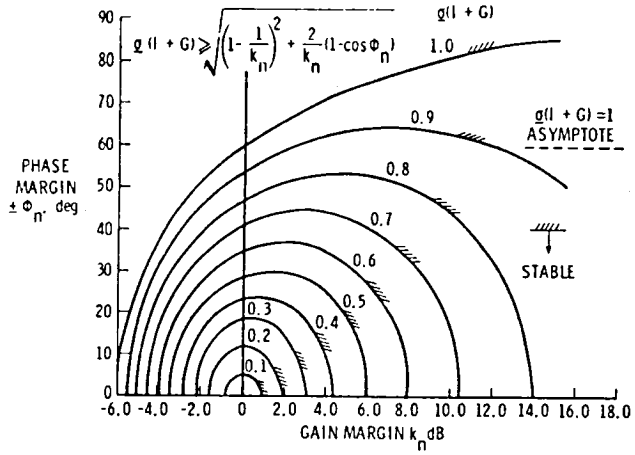

Fig. 3 Regions of guaranteed stability for various minimum singular value $\underline{\sigma}$ (I+G).

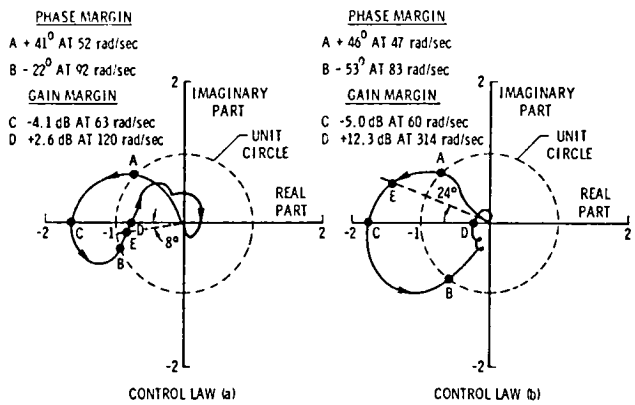

Fig. 4 Nyquist diagrams of 29th order flutter suppression system from ref. 7 (arrows indicate increasing frequency).

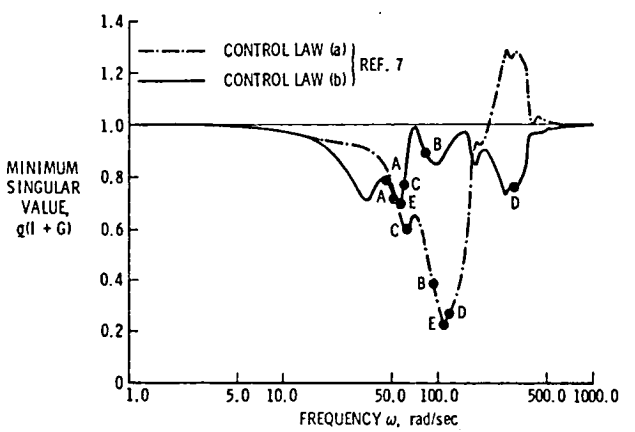

Fig. 5 Minimum singular value variation with frequency for 29th order flutter suppression system.

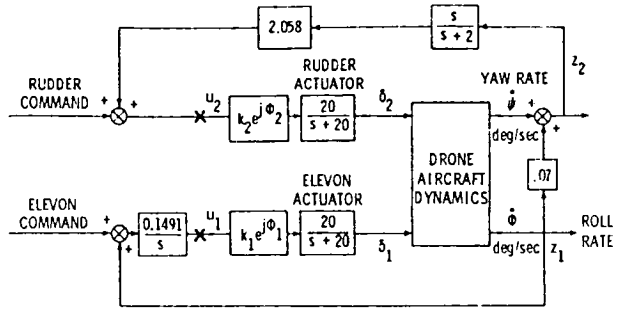

Fig. 6 Block diagram of a drone lateral attitude control system.

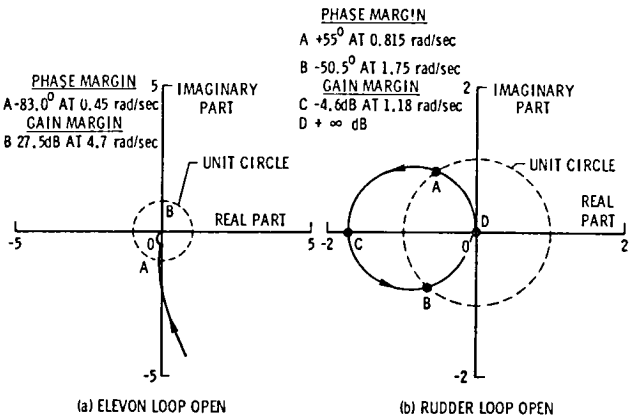

Fig. 7 Nyquist diagrams from single loop breaking tests (drone lateral attitude control system).

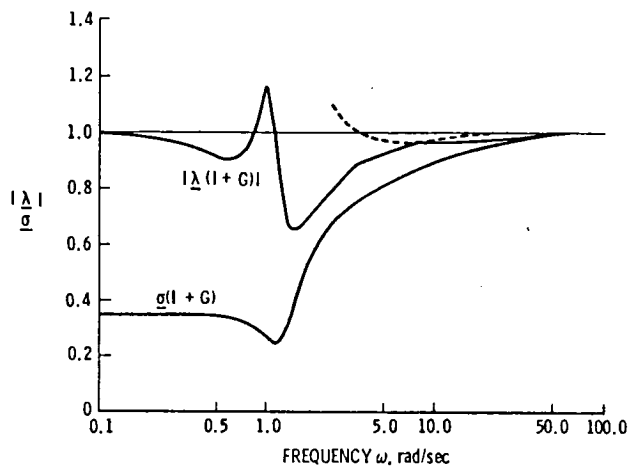

Fig. 8 Variation of minimum singular value ($\underline{\sigma}$) and minimum eigenvalue ($|\underline{\lambda}|$) of (I+G) with frequency (drone lateral attitude control system).

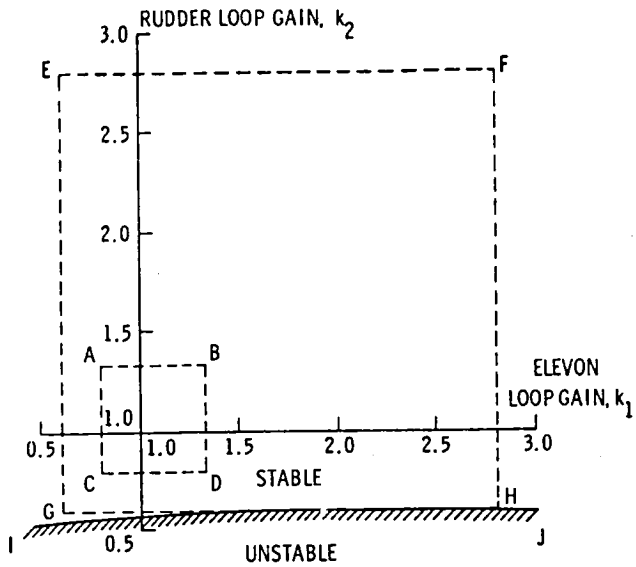

Fig. 9 Stability boundary with respect to loop gain change at input based on (a) minimum singular value - ABDC, (b) minimum eigenvalue - EFHG, and (c) actual stability boundary - IJ.

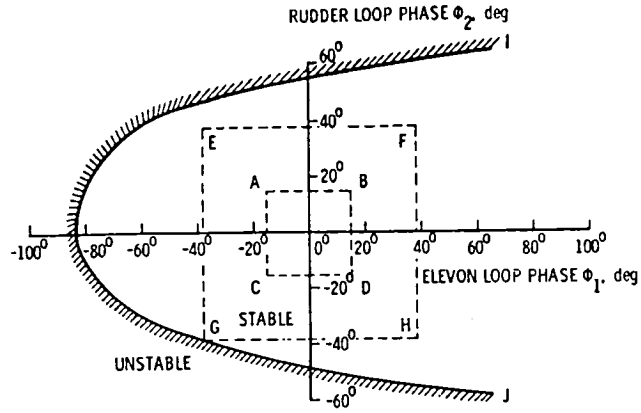

Fig. 10 Stability boundary with respect to loop phase change at input based on (a) minimum singular value - ABDC, (b) minimum eigenvalue - EFHG, and (c) actual stability boundary - IJ.

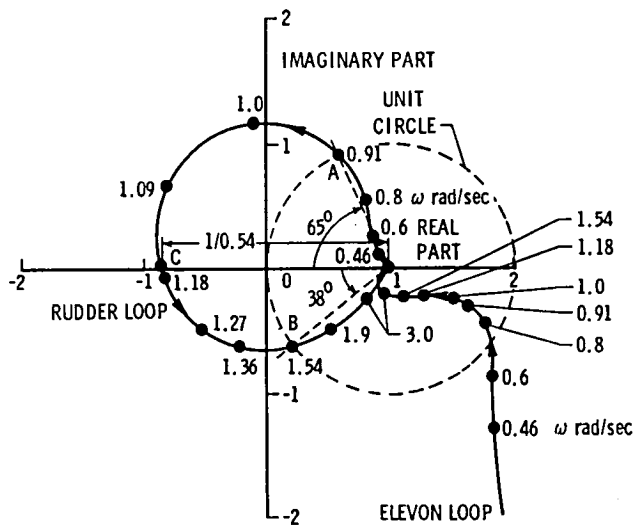

Fig. 11 Polar plot of eigenvalues of return difference matrix $\lambda(I+G)$ variation with frequency (drone lateral attitude control system).

1 Report No	2 Government Accession No.	3. Recipient's Catalog No.
NASA TM-84524		

4 Title and Subtitle	5. Report Date
Application of Matrix Singular Value Properties for Evaluating Gain and Phase Margins of Multiloop Systems	July 1982
	6. Performing Organization Code 505-33-63-03

7 Author(s)	8. Performing Organization Report No.
V. Mukhopadhyay of George Washington University and J. R. Newsom of NASA Langley Research Center	
	10. Work Unit No.
9. Performing Organization Name and Address	
NASA Langley Research Center Hampton, VA 23665	11. Contract or Grant No.
	13. Type of Report and Period Covered Technical Memorandum
12. Sponsoring Agency Name and Address	
National Aeronautics and Space Administration Washington, DC 20546	14. Sponsoring Agency Code

15. Supplementary Notes
Presented at the AIAA Guidance and Control Conference
August 9-11, 1982
San Diego, California
AIAA Paper 82-1574

16. Abstract

A stability margin evaluation method in terms of simultaneous gain and phase changes in all loops of a multiloop system is presented. A universal gain-phase margin evaluation diagram is constructed by generalizing an existing method using matrix singular value properties. Using this diagram and computing the minimum singular value of the system return difference matrix over the operating frequency range, regions of guaranteed stability margins can be obtained. Singular values are computed for a wing flutter suppression and a drone lateral attitude control problem. The numerical results indicate that this method predicts quite conservative stability margins. In the second example if the eigenvalue magnitude is used instead of the singular value, as a measure of nearness to singularity, more realistic stability margins are obtained. However, this relaxed measure generally cannot guarantee global stability.

17. Key Words (Suggested by Author(s))	18. Distribution Statement
Multivariable control systems Robustness Singular-value-decomposition	Unclassified - Unlimited Star Category - 63

19. Security Classif. (of this report)	20. Security Classif. (of this page)	21. No. of Pages	22. Price
Unclassified	Unclassified	10	A02